Journal of Experimental Botany, Vol. 71, No. 20 pp. 6524–6537, 2020
doi:10.1093/jxb/eraa356 Advance Access Publication 29 July 2020

RESEARCH PAPER

Nutrition-mediated cell and tissue-level anatomy triggers the covariation of leaf photosynthesis and leaf mass per area

Zhifeng Lu[1,2], Tao Ren[1,2], Jing Li[1,2], Wenshi Hu[1,2], Jianglin Zhang[1,2], Jinyao Yan[1,2], Xiaokun Li[1,2], Rihuan Cong[1,2], Shiwei Guo[3] and Jianwei Lu[1,2,*],

[1] Microelement Research Center, Huazhong Agricultural University, Wuhan 430070, China
[2] Key Laboratory of Arable Land Conservation (Middle and Lower Reaches of Yangtze River), Ministry of Agriculture and Rural Affairs, Wuhan 430070, China
[3] Jiangsu Provincial Key Lab for Organic Solid Waste Utilization, National Engineering Research Center for Organic-based Fertilizers, Nanjing Agricultural University, Nanjing 210095, China

* Correspondence: lunm@mail.hzau.edu.cn

Received 22 July 2020; Accepted 22 July 2020

Editor: Christine Raines, University of Essex, UK

Abstract

Plants in nutrient-poor habitats converge towards lower rates of leaf net CO_2 assimilation (A_{area}); however, they display variability in leaf mass investment per area (LMA). How a plant optimizes its leaf internal carbon investment may have knock-on effects on structural traits and, in turn, affect leaf carbon fixation. Quantitative models were applied to evaluate the structural causes of variations in LMA and their relevance to A_{area} in rapeseed (*Brassica napus*) based on their responses to nitrogen (N), phosphorus (P), potassium (K), and boron (B) deficiencies. Leaf carbon fixation decreased in response to nutrient deficiency, but the photosynthetic limitations varied greatly depending on the deficient nutrient. In comparison with A_{area}, the LMA exhibited diverse responses, being increased under P or B deficiency, decreased under K deficiency, and unaffected under N deficiency. These variations were due to changes in cell- and tissue-level carbon investments between cell dry mass density (N or K deficiency) and cellular anatomy, including cell dimension and number (P deficiency), or both (B deficiency). However, there was a conserved pattern independent of nutrient-specific limitations—low nutrient availability reduced leaf carbon fixation but increased carbon investment in non-photosynthetic structures, resulting in larger but fewer mesophyll cells with a thicker cell wall but a lower chloroplast surface area appressed to the intercellular airspace, which reduced the mesophyll conductance and feedback-limited A_{area}. Our results provide insight into the importance of mineral nutrients in balancing the leaf carbon economy by coordinating leaf carbon assimilation and internal distribution.

Keywords: Carbon investment, leaf anatomy, leaf carbon economy, leaf dry mass per unit leaf area, leaf photosynthesis, nutrient deficiency.

Abbreviations: A_{area}, light-saturated photosynthetic rate per unit leaf area; A_{mass}, light-saturated photosynthetic rate per unit mass; AF_{pa}, airspace fraction of the palisade mesophyll layers; AF_{sp}, airspace fraction of the spongy mesophyll layers; α, leaf absorbance; β, fraction of light absorbed by PSII; CV, mean cell volume; CV_{pa}, volume of palisade mesophyll cells; CV_{sp}, volume of spongy mesophyll cells; D_L, dry mass density; Γ^*, CO_2 compensation point; g_m, mesophyll conductance to CO_2; g_s, stomatal conductance to H_2O; g_{sc}, stomatal conductance to CO_2; J_f, linear electron transport rate on the basis of chlorophyll fluorescence; J_{max}, the maximal rate of electron transport; J_{1200}, potential electron transport rate at PPFD of 1200 μmol m^{-2} s^{-1}; $l_m/A_{section}$, length of mesophyll exposed to intercellular airspace per cross-sectional area; LMA, dry mass per unit leaf area; NCA, number of cells per leaf area; NCL, number of cell layers; NCL_{pa}, number of palisade mesophyll cell layers; NCL_{sp}, number of spongy mesophyll cell layers; PPFD, photosynthetic photon flux density; R_d, day respiration rate; ρ_{cell}, average bulk cell dry mass density across epidermis and mesophyll tissues; ρ_{tc}, average dry mass density of the upper and lower cuticle; Φ_{PSII}, actual photochemical efficiency of photosystem II; S_c, chloroplast surface area exposed to intercellular airspace; S_m, mesophyll surface area exposed to intercellular airspace; T_{cw}, cell wall thickness; T_L, leaf thickness; TMA_V, vein mass per leaf area; V_{cmax}, maximum rate of RuBP carboxylation; VPA, non-airspace volume of the tissue per leaf area.

Introduction

Deleterious effects on plant productivity due to nutrient limitation are widespread, particularly from a lack of essential elements and some micronutrients (Alloway, 2008; Ellsworth *et al.*, 2015; Sardans and Peñuelas, 2015). Nutrient deprivation retards light-saturated photosynthetic rate per unit leaf area (A_{area}) in green leaves and impacts the subsequent investment of assimilates (Jákli *et al.*, 2017; Tränkner *et al.*, 2018; Xiong and Flexas, 2018; Lu *et al.*, 2019). However, the carbon investment used for leaf establishment is more complex as leaf mass per area (LMA) can either increase or decrease in leaves deprived of mineral nutrients. For instance, LMA was found to be increased in nitrogen (N)-deprived *Oryza sativa* L. leaves (Xiong *et al.*, 2015) and boron (B)-deficient *Gossypium hirsutum* L. leaves (Zhao and Oosterhuis, 2002) but decreased in *Oryza sativa* L. leaves under potassium (K) deficiency (Xie *et al.*, 2020). As two key traits, A_{area} and LMA are crucial for balancing the carbon economy in plants, representing carbon acquisition and investment per unit leaf area, respectively (Wright *et al.*, 2002). The trade-off expressed by the combination of these traits is an indicator of the strategies employed by plants to adapt to the prevailing environmental conditions, which largely underpin the worldwide 'leaf economics spectrum' (Wright et al., 2004). Leaves under nutrient deficiencies tends to have a lower carbon fixation capacity but display diversity in carbon investment per unit leaf area, which indicates the possibility of different adaptations to nutrient-poor habitats within or across species. However, little is known about this possibility and the underlying driving forces.

To achieve real progress in understanding how plants cope with nutrient deficiencies from the point of view of the leaf carbon economy, we must assess the strategy of carbon allocation to leaves at different physiological or structural levels (i.e. a comprehensive analysis of the compositional basis of LMA). Prior studies have broken the LMA down into leaf thickness (T_L) and dry mass density (D_L), with LMA=T_L×D_L (Witkowski and Lamont, 1991), and determined the predominant driver of variations in LMA. According to comparisons of LMA across grasses, herbaceous dicots, deciduous species, and evergreen woody species, Poorter *et al.* (2009) concluded that D_L explained 80% of the difference in LMA, which was consistent with the observations in rice (Xiong *et al.*, 2016). However, LMA has also been reported to be driven mainly by T_L (Vile *et al.*, 2005), or equally by D_L and T_L (Villar *et al.*, 2013). Therefore, it is difficult to understand leaf carbon economics based on these gross structural traits because D_L and T_L can have opposite effects on LMA. By partitioning LMA as the sum of the tissue mass of different cellular components or proposing models based on the hypothesis that LMA is driven by anatomical traits (e.g. mesophyll cell volume and number, airspace fraction, or leaf vein trait), previous studies have shown that high-LMA species often show a higher leaf tissue density and larger cell sizes (Sack *et al.*, 2003; Shipley *et al.*, 2006; Poorter *et al.*, 2009; Blonder *et al.*, 2011; Villar *et al.*, 2013; John *et al.*, 2017). Lack of nutrients retards leaf growth through a set of influences on tissue- and cell-level properties, including regulation of cell number and volume by mediating cell division and expansion (Marschner, 2012; Müller *et al.*, 2015) and cell wall and cellular composition by mediating metabolic fluxes (Amtmann and Armengaud, 2009; Poorter *et al.*, 2009). However, these influences are not consistent among different types of nutrient deficiencies. For instance, N deficiency increases cell wall thickness of rice by up-regulating carbon flow to structural carbohydrates, but sufficient N is favourable to the enlargement of chloroplasts (Li *et al.*, 2009; Ali and Golombek, 2016); mesophyll cell size tends to increase in phosphorus (P)- and B-poor orange leaves but decreases in *Eucalyptus grandis* leaves suffering from K deficiency (Battie-Laclau *et al.*, 2014; Liu *et al.*, 2014). In this sense, nutrition-mediated variations in LMA may be effectively reflected by integration of anatomical traits even when leaves under different nutrient starvation conditions have similar LMA shifts, indicating the possible carbon allocation strategies during adaptation.

Leaf carbon-fixation capacity, as another factor in balancing the plant carbon economy, determines the carbon flux available for subsequent leaf establishment. Different nutrient deficiencies may result in diverse leaf carbon flow rates and lead to variations in the distribution of carbon at the cell and tissue level. Carbon allocations, including alterations in cell wall thickness, mesophyll cell size, and chloroplast density, may also synchronously influence leaf internal CO_2 diffusion, and, in turn, regulate photosynthesis (Terashima *et al.*, 2011; Tosens *et al.*, 2012; Tomás *et al.*, 2013; Lundgren and Fleming, 2020). Given this interplay between leaf carbon acquisition and investment, it is not surprising that both processes are tightly co-regulated. Nutrient supply is known to affect leaf anatomy by mediating internal carbon distribution; however, the available research has not dissected out the influence of different nutrients on leaf cell- and tissue-level properties and the subsequent consequences for leaf function. Also, the role of nutrient elements in modulating the co-regulation of leaf carbon fixation and investment, particularly considering the structural trade-offs, which may trigger different adaptations to the prevailing nutrient deficiency, is unclear. Therefore, we hypothesized that nutrient-induced variations on an anatomical and compositional basis may underpin the covariation of A_{area} and LMA, allowing the leaf to cope with variable nutrient stresses.

Winter oilseed rape (*Brassica napus* L.) is a herbaceous annual plant that requires large amounts of N (147–333 kg ha^{-1}; Ren and Lu, 2016), P (29.6–77.9 kg ha^{-1}; Li *et al.*, 2011), and K (290–373 kg ha^{-1}; Orlovius, 2003) during the growth period. Deficiencies in these nutrients decrease seed yield. Additionally, rapeseed is extremely sensitive to B deficiency and will flower without seed setting when B is insufficient, reducing yields. Therefore, we examined the effects of a variety of parameters on carbon assimilation and investment and the cellular and tissue anatomy in rapeseed under N-, P-, K- and B-deficient conditions. The aims were: (i) to verify the possibility of different adaptations within a single species to nutrient-poor conditions by considering cell- and tissue-level carbon trade-offs, (ii) to evaluate the influence of nutrition-mediated structural properties on leaf carbon fixation, and (iii) to identify the anatomical basis of adjustments in A_{area} and LMA.

Materials and methods

Study site and growth conditions

The field experiment was conducted during the 2017–2018 rapeseed growing season in Wuxue County, Hubei Province, China (30°06′46″N, 115°36′9″E). The site has a subtropical monsoon climate and receives 877 mm of precipitation annually, with a mean temperature of 13.8 °C during the growth period. The field soil was a sandy loam of pH 5.1 (1:2.5 soil: deionized water), with organic matter 32.3 g kg^{-1}, total N 1.8 g kg^{-1}, NH_4OAc-K 49.8 mg kg^{-1}, Olsen-P 13.1 mg kg^{-1}, and hot-water-soluble B 0.25 mg kg^{-1} in the topsoil layer (0–20 cm).

Experimental design

A complete randomized block design was carried out with five treatments and four replications. The treatments were: (i) control treatment (CK), with recommended fertilizer application for this region (180 kg N ha^{-1}, 90 kg P_2O_5 ha^{-1}, 120 kg K_2O ha^{-1}, and 1.6 kg B ha^{-1}); (ii) N deficiency; (iii) P deficiency; (iv) K deficiency; and (v) B deficiency. In the N-, P-, K-, and B-deficient treatments, the appropriate nutrient was omitted. N (urea, 46% N) was applied in three splits: 60% as basal fertilizer, i.e. Biologische Bundesantalt, Bundessortenamt and Chemische Industrie (BBCH) 15–16 (Lancashire *et al.*, 1991), 20% during the overwintering stage (BBCH 29) and 20% at the beginning of stem elongation (BBCH 30). P (superphosphate, 12% P_2O_5), K (potassium chloride, 60% K_2O), B (borax, 10.8%) fertilizers were applied manually as basal fertilizers. The plot was of 20 m^2, with a length of 10 m and a width of 2 m.

Rapeseed seedlings were sown and grown in a nursery for approximately 4 weeks and were transplanted at the five- to six-leaf stage (BBCH 15–16) on 6 November 2017 in double rows spaced approximately 0.3 m apart, with 0.2–0.3 m between plants, corresponding to 112 500 plants ha^{-1}. The seedlings were grown under rain-fed conditions. Commercial herbicides, insecticides, and fungicides were applied, and no visual symptoms of disease were observed during the growth season.

Leaf morphology and nutrient concentrations

Eighty days after the transplanting, plants within the same treatment had grown consistently among different replicates. To obtain better estimates of agronomic traits (such as seed yield at maturity), one of the four replicates was not used for whole-plant destructive sampling. Therefore, plants and third fully expanded leaves (from apex downwards) were randomly sampled from three of the four replicate plots to determine plant biomass, leaf morphological traits and nutrient concentration (N, P, K, B). Leaf area was measured using Image-Pro Plus 4.5 software (Media Cybernetics, Silver Spring, MD, USA). Leaf thickness was determined using a digital thickness gauge (model 547-401; Mitutoyo, Kawasaki, Japan); care was taken to avoid the midrib during measurement. For a given leaf, the thickness of leaf tip, center and base were measured and then averaged. The LMA was determined by dividing the leaf dry mass by the surface area, and the leaf density was obtained by dividing the LMA by the leaf thickness (Witkowski and Lamont, 1991). Dried leaves were milled and digested with H_2SO_4–H_2O_2 to determine the N, P, and K concentrations (Thomas *et al.*, 1967), and dry-ashed at 500 °C for 4 h and suspended in 0.1 M HCl to determine the B concentration (Dible *et al.*, 1954).

Leaf cross-sectional anatomy

Pieces (1–2 mm^2) cut from the middle of the leaves (avoiding midvein and secondary veins, Fig. 1) were fixed under vacuum in 2.5% glutaraldehyde (v/v) in 0.1 M phosphate buffer (pH 7.4) for 4 h. Then they were washed and post-fixed in 2% osmium tetroxide at 4 °C for 4 h. Afterwards, the samples were dehydrated in an ethanol series (10–100%) and propylene oxide, and embedded in Epon 812 resin. Semi-thin (1 μm) and ultrathin (90 nm) cross sections were cut with an LKB-5 ultramicrotome (LKB Co., Ltd, Uppsala, Sweden). The semi-thin cross sections were stained with toluidine blue and photographed at ×200 magnification with a Nikon 5 MP digital microscope camera DS-Fi1 (Nikon Corp., Kyoto, Japan). The ultrathin sections were examined with a transmission electron microscope (H-750; Hitachi, Tokyo, Japan) after staining with 2.0% uranyl acetate (w/v) and lead citrate. Micrographs were captured at magnifications of ×2000–3000 to observe the distribution of chloroplasts and ×20 000–40 000 for the measurement of cell wall thickness. To avoid the possible effects of poor staining and blurred imaging during the slicing process on the effective observations, we added one leaf segment from the fourth replicate, i.e. we used four leaves each from a different field replicate to prepare cross sections and take photographs. Measurements of the cross-sectional anatomy were performed using Image-Pro Plus 4.5 software.

The mesophyll (S_m) and chloroplast surface area exposed to intercellular airspace per unit leaf area (S_c) was calculated according to Syvertsen *et al.* (1995):

$$S_m = \frac{l_m}{W} F \quad (1)$$

$$S_c = \frac{l_c}{l_m} S_m \quad (2)$$

where W is the width of leaf cross section, and l_m and l_c are the total lengths of the mesophyll cell wall and chloroplast touching the plasma membrane appressed to the intercellular air space, respectively. The curvature correction factor (F) that allows cross-section lengths to be converted to surface area was determined by assuming the palisade and spongy cells as capsules (Thain, 1983; Harwood *et al.*, 2020). F was calculated for each leaf from the average ratio of cell width to height for palisade and spongy cells (1.37 for the control and N deficiency treatments, 1.39 for the P and K deficiency treatments and 1.41 for the B deficiency treatment). The length of mesophyll exposed to intercellular airspace per cross-sectional area ($l_m/A_{section}$) was calculated by dividing l_m by the total cross-sectional area according to Nelson *et al.* (2005). The fraction of the intercellular air space of the mesophyll (AF), spongy (AF_{sp}), and palisade (AF_{pa}) layers was determined by dividing the corresponding cross-sectional area of the intercellular air space by the area of mesophyll tissue. The average cell cross-sectional area, cell height of epidermis, palisade, and spongy cells, cell diameter and perimeter, cell aspect ratio, and number of layers of epidermal, spongy, and palisade cells were determined as described in John *et al.* (2017). These parameters were analysed in at least three different fields of view for each leaf cross section.

Assessing the drivers of differences in LMA between nutrient deficiency and control treatments

We applied the Exhaustive Anatomy and Composition of Tissues (EXACT) approach proposed by John *et al.* (2017) to assess the influence of anatomical traits on variations in LMA between the nutrient deficiency and control treatments. Briefly, for a given leaf, the LMA is the sum of the tissue mass of each component:

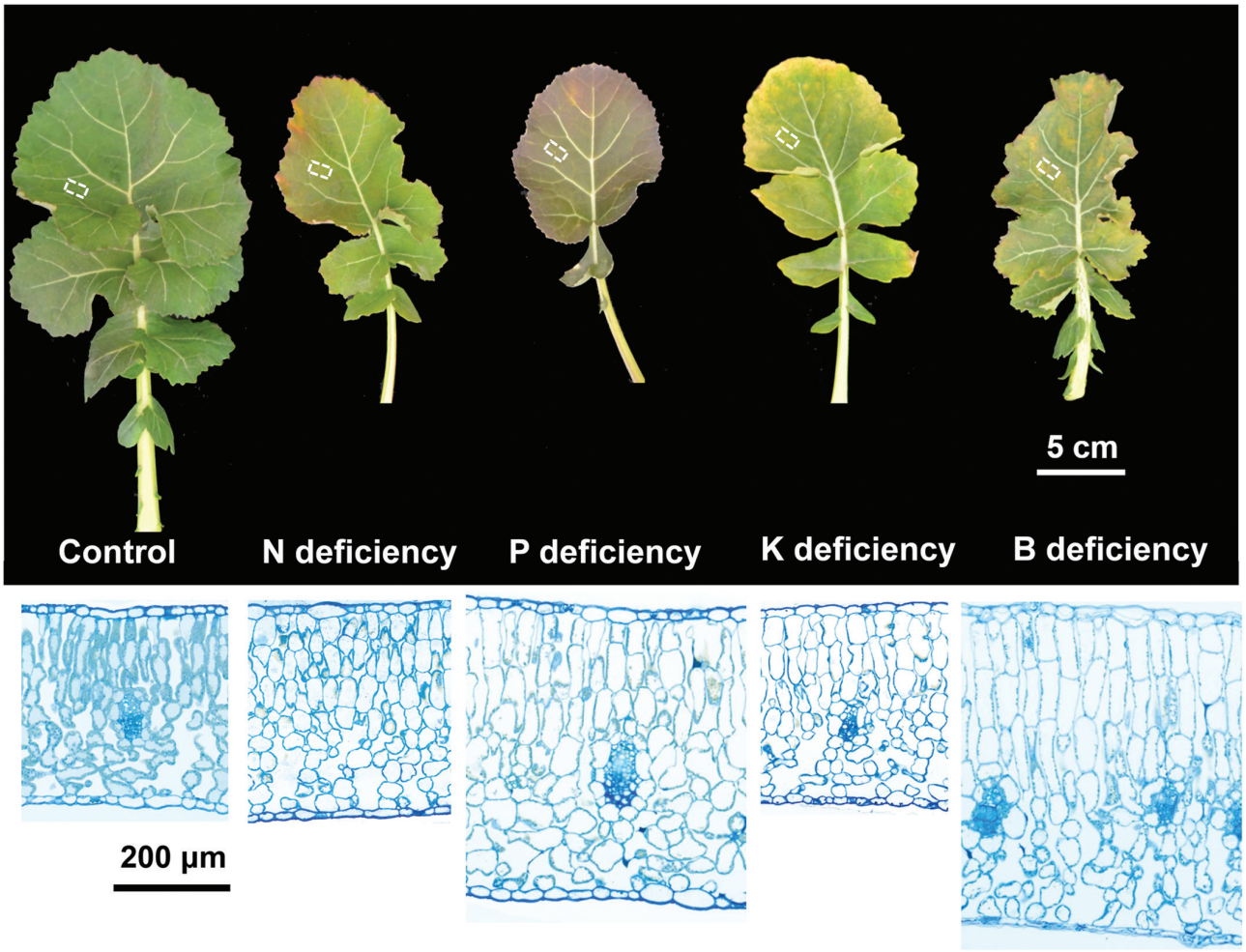

Fig. 1. Leaf symptoms (scale bar: 5 cm) and representative light micrographs (scale bar: 200 μm) of leaf cross sections of control and nutrient deficiency treatments in rapeseed under field conditions. The dashed boxes show where leaves were sampled for anatomical analysis. (This figure is available in color at *JXB* online.)

$$\begin{aligned} LMA = &\left(CV_{ue}\left(NCA_{ue}\right) + CV_{pa}\left(NCA_{pa}\right)\right. \\ &\left. + CV_{sp}\left(NCA_{sp}\right) + CV_{le}\left(NCA_{le}\right)\right)\rho_{cell} \\ &+ \left(VPA_{uc} + VPA_{lc}\right)\rho_{tc} + TMA_V \end{aligned} \quad (3)$$

where the subscripts ue, pa, sp, le, uc, and lc represent, respectively, the upper epidermis, palisade mesophyll, spongy mesophyll, lower epidermis, upper cuticle, and lower cuticle. CV is the mean estimated cell volume and NCA is the number of cells per leaf area. VPA is the non-airspace volume of the tissue per leaf area. ρ_{cell} is the average bulk cell dry mass density across epidermis and mesophyll tissues, and ρ_{tc} is the average dry mass density of the upper and lower cuticle, which was assumed to be constant (1.17 kg m^{-3}) as in John *et al.* (2017). TMA_V is the vein mass per leaf area. Given the lack of data on TMA_V during the 2017–2018 growing season, we used the values from leaves in the same position during the 2019–2020 growing season to evaluate the influence of different nutrient deficiencies on vein mass accumulation. Rapeseed plants from two growing seasons were at the same growth stage (overwintering stage) and the sampled leaves were similar in biomass, area, and LMA (see Supplementary Table S1; Supplementary Protocol S1 at *JXB* online). Since the leaf traits were not exactly the same between the two years and any variations may result in different outputs of the model, we performed a sensitivity analysis by using ±5% deviation of the TMA_V to improve the confidence in the quantitative calculations (Supplementary Table S2). The results indicated that the deviation of TMAv has a marginal influence on the contribution of each compositional traits to LMA variation under nutrient deficiency. Equation 3 can be rearranged to enable ρ_{cell} to be calculated from the measured LMA and anatomical traits:

$$\rho_{cell} = \frac{LMA \times \left(1 - \frac{\left(VPA_{uc}+VPA_{lc}\right)\rho_{tc}}{LMA}\right) - TMA_V}{CV_{ue}\left(NCA_{ue}\right) + CV_{pa}\left(NCA_{pa}\right) + CV_{sp}\left(NCA_{sp}\right) + CV_{le}\left(NCA_{le}\right)} \quad (4)$$

VPA_{tc} (the sum of VPA_{uc} and VPA_{lc}) was calculated by assuming that the cuticle thickness was on average 3.6% of the total leaf thickness (John *et al.*, 2013). The CV of each tissue could be modelled by assuming epidermal cells as cylinders, palisade and spongy mesophyll cells as capsules; this required determination of the cell diameter and height (Chatelet *et al.*, 2013; John *et al.*, 2017; Harwood *et al.*, 2020). For palisade

and spongy mesophyll cells, the NCA can be determined as the total VPA minus the volume per unit area of the airspace divided by the CV. The total VPA of a tissue x is calculated as:

$$\mathrm{VPA_x} = \mathrm{CH_x} \times \mathrm{NCL_x} \tag{5}$$

where $\mathrm{CH_x}$ is the mean cell height and $\mathrm{NCL_x}$ is the number of cell layers.

We compared the mean LMA in plants under the nutrient deficiency and control treatments, and its underlying compositional basis, by evaluating the airspace fraction of the palisade and spongy mesophyll layers ($\mathrm{AF_{pa}}$ and $\mathrm{AF_{sp}}$), $\mathrm{CV_x}$, $\mathrm{NCL_x}$, ρ_{cell}, and $\mathrm{TMA_V}$.

Determination of contributions of variables to LMA changes

We examined contributions to changes in the leaf LMA related to variations in the contributing factors by quantifying differences in plant traits between the control (CK) and nutrient deficiency (ND) treatments, using the approach of Buckley and Diaz-Espejo (2015*a*). This method is based on an infinitesimal change in LMA equal to the sum of infinitesimal changes in the underlying variables:

$$\begin{aligned} d\mathrm{LMA} &= \frac{\partial \mathrm{LMA}}{\partial x_1} dx_1 + \frac{\partial \mathrm{LMA}}{\partial x_2} dx_2 + \cdots + \frac{\partial \mathrm{LMA}}{\partial x_n} dx_n \\ &= \sum_j \frac{\partial \mathrm{LMA}}{\partial x_j} dx_j \end{aligned} \tag{6}$$

To apply Eqn 6, this expression is integrated over the interval of each variable between the CK and ND treatments, which gives the finite difference in LMA, δLMA, between the two treatments:

$$\delta\mathrm{LMA} = \int_{\mathrm{CK}}^{\mathrm{ND}} \frac{\partial \mathrm{LMA}}{\partial x_1} dx_1 + \int_{\mathrm{CK}}^{\mathrm{ND}} \frac{\partial \mathrm{LMA}}{\partial x_2} dx_2 + \cdots = \sum_j \int_{\mathrm{CK}}^{\mathrm{ND}} \frac{\partial \mathrm{LMA}}{\partial x_j} dx_j \tag{7}$$

The integrals can be estimated numerically by approximating the differentials and derivatives therein as finite differences and ratios of the finite differences, respectively. Taking the term with x_1 as an example:

$$\begin{aligned} \int_{\mathrm{CK}}^{\mathrm{ND}} \frac{\partial \mathrm{LMA}}{\partial x_1} dx_1 &\approx \sum_{k=0}^{t-1} \left(\frac{\Delta \mathrm{LMA}}{\Delta x_1} \middle| \begin{matrix} k, k+1 \\ x_2, \ldots x_n \end{matrix} \right) \cdot \Delta x_1 \\ &= \sum_{k=0}^{t-1} \left(\Delta \mathrm{LMA} \middle| \begin{matrix} k, k+1 \\ x_2, \ldots x_n \end{matrix} \right) \end{aligned} \tag{7a}$$

where t denotes the number of sub-intervals between the CK and ND (k=0 and t, respectively), and numerical integration with t=1000 is adequate and feasible (Buckley and Diaz-Espejo, 2015*a*). The superscript 'k, k+1' means that the changes in ΔLMA and Δx_1 are computed between indices k and k+1; and the subscript 'x_2, … x_n' indicates that ΔLMA is computed by changing x_1 while holding x_2, … x_n constant. A more simplified and generalized notation is this:

$$\int_{\mathrm{CK}}^{\mathrm{ND}} \frac{\partial \mathrm{LMA}}{\partial x_1} dx_1 \approx \sum_{k=0}^{t-1} \left[\delta\mathrm{LMA} \middle| \delta x_1 \right]_k^{k+1} \tag{7b}$$

On the right-hand side of Eqn 7b, variables after the vertical bar are allowed to change, and all other variables are held constant. The other terms of Eqn 7 (those involving x_2, … x_n) are integrated using the same method. The numerical integration in Eqn 7 requires an assumption about how x_1, x_2, … x_n vary across the interval. For simplicity, we assumed that the variables change at a uniform rate across the interval between CK and ND. For example, at a given point in the interval, x_1 might be 10% of the way from its value in ND to its value in CK, and the same is true for x_2 and all of the other variables. These numerical procedures were performed using worksheets and user-defined functions and Visual Basic for Applications subroutines in a Microsoft Excel spreadsheet. A detailed computer code example can be obtained from 'Supporting Information Note S2' of Buckley and Diaz-Espejo (2015*a*).

A completed integral denotes the absolute contribution of a variable to the total change in LMA:

$$\begin{aligned} \delta\mathrm{LMA} = \; & \delta\mathrm{LMA}\,(\text{due to } x_1) \\ & + \delta\mathrm{LMA}\,(\text{due to } x_2) + \cdots + \delta\mathrm{LMA}\,(\text{due to } x_n) \end{aligned} \tag{8}$$

Then, the contribution from a variable x_j ($\mathrm{AF_{pa}}$, $\mathrm{AF_{sp}}$, $\mathrm{CV_x}$, $\mathrm{NCL_x}$, ρ_{cell} and $\mathrm{TMA_V}$) to a change in LMA is defined as:

$$\rho_{xj} = 100 \cdot \frac{\delta\mathrm{LMA}\,(\text{due to } x_j)}{\delta\mathrm{LMA}} \tag{9}$$

Gas exchange and fluorescence measurements

Measurements were conducted on fully expanded leaves (the third leaves from the apex downwards) using a LI-6400 portable photosynthesis system equipped with a 2 $\mathrm{cm^2}$ LI-6400–40 chamber (LI-COR Inc., Lincoln, NE, USA). The leaves were stabilized in the chamber at a temperature of 15 °C, a relative humidity of 40–50%, a $\mathrm{CO_2}$ concentration (C_a) of 400 μmol $\mathrm{mol^{-1}}$, and a photosynthetic photon flux density (PPFD) of 1200 μmol $\mathrm{m^{-2}\ s^{-1}}$ (10: 90% blue: red light). After reaching a steady state, the gas exchange parameters, fluorescence yield (F_s), and maximum fluorescence (F_m') were recorded. Given that the calculation of mesophyll conductance to $\mathrm{CO_2}$ (g_m) involves many assumptions and limitations that may reduce the accuracy and repeatability, resulting in large standard deviations (Warren, 2006), four leaves each from a different replicate plot were used for estimation. Then three of them were randomly selected to measure $\mathrm{CO_2}$ response curves at a PPFD of 1200 μmol $\mathrm{m^{-2}\ s^{-1}}$. First, C_a was decreased stepwise from

400 to 50 μmol mol^{-1}; it was then increased to 400 μmol mol^{-1} until the original A_{area} was achieved. Next, C_a was increased from 400 to 1800 μmol mol^{-1}. In all cases, measurements of A_{area} were recorded after the gas-exchange rate had stabilized at a given C_a. The actual photochemical efficiency of photosystem II (Φ_{PSII}) was calculated:

$$\Phi_{PSII} = \frac{F'_m - F_s}{F'_m} \tag{10}$$

The linear electron transport rate on the basis of chlorophyll fluorescence (J_f) was computed as:

$$J_f = \Phi_{PSII} PPFD\ \alpha\beta \tag{11}$$

where α is the leaf absorbance and β is the fraction of light absorbed by PSII. Their product was estimated from the relationship between Φ_{PSII} and Φ_{CO_2} from the photosynthetic light-response curves under non-photorespiratory conditions in a low O_2 (<2%) atmosphere according to Valentini *et al.* (1995). Briefly, light responses curves were carried out at <2% O_2 on the same leaves used for gas exchange measurement by progressively decreasing PPFD from 1500 to 300 μmol m^{-2} s^{-1} (see Supplementary Fig. S1). This allowed the calculation of Φ_{CO_2} as:

$$\Phi_{CO_2} = \frac{4 \times (A_{area} + R_d)}{PPFD} \tag{12}$$

where R_d is the day respiration rate, which was assumed to be half of the dark respiration rate. The g_m and the chloroplastic CO_2 concentration (C_c) were calculated based on the variable J method (Harley *et al.*, 1992):

$$g_m = \frac{A_{area}}{C_i - \frac{\Gamma^*(J_f + 8(A_{area} + R_d))}{J_f - 4(A_{area} + R_d)}} \tag{13}$$

$$C_c = C_i - \frac{A_{area}}{g_m} \tag{14}$$

where C_i is the intercellular CO_2 concentration and Γ⋆ is the CO_2 compensation point in the absence of mitochondrial respiration. A Γ⋆ typical for rapeseed, 40.6 μmol mol^{-1}, was used in this study (Lu *et al.*, 2016).

According to the Farquhar, von Caemmerer and Berry (FvCB) model, the net photosynthetic rate is limited mainly by Rubisco carboxylation or by RuBP regeneration (Farquhar *et al.*, 1980). Therefore, we calculated the maximum rate of RuBP carboxylation (V_{cmax}) and the maximal rate of electron transport (J_{max}) at measurement temperature using the 'fitacis' function of the 'plantecophys' package (Duursma, 2015). Since there is no way to ensure the PPFD (1200 μmol m^{-2} s^{-1}) was truly saturating for all CO_2 response curves, J_{max} is reported as the potential electron transport rate at PPFD of 1200 μmol m^{-2} s^{-1} (J_{1200}; Buckley and Diaz-Espejo, 2015*b*). We performed fits using A_{area}, C_i, PPFD, leaf temperature, measured g_m, and R_d as inputs. Other settings were left at default, as these should have a limited impact on the objective of this study (comparing the differences between parameters obtained from different nutrient treatments). The sensitivity of A_{area} to underlying variables was calculated to analyse the influence of individual traits on the differences in A_{area} caused by nutrient deficiency. The absolute change in A_{area} was partitioned into contributions from diffusion (stomatal conductance to CO_2 (g_{sc}) and g_m) and biochemical parameters (J_{1200}, V_{cmax}, and R_d) using the aforementioned method used for partitioning changes in LMA. Briefly, an infinitesimal change in A_{area} is assumed to be equal to the sum of infinitesimal changes in the following variables:

$$dA_{area} = \frac{\partial A_{area}}{\partial g_{sc}} dg_{sc} + \frac{\partial A_{area}}{\partial g_m} dg_m + \frac{\partial A_{area}}{\partial J_{1200}} dJ_{1200} + \frac{\partial A_{area}}{\partial V_{cmax}} dV_{cmax} + \frac{\partial A_{area}}{\partial R_d} dR_d \tag{15}$$

Integrating this expression over the interval of each variable between the control and nutrient deficiency treatments gives the finite difference in A_{area}:

$$\delta A_{area} = \int_{ND}^{CK} \frac{\partial A_{area}}{\partial g_{sc}}\ dg_{sc} + \int_{ND}^{CK} \frac{\partial A_{area}}{\partial g_m}\ dg_m + \int_{ND}^{CK} \frac{\partial A_{area}}{\partial J_{1200}}\ dJ_{1200} + \int_{ND}^{CK} \frac{\partial A_{area}}{\partial V_{cmax}}\ dV_{cmax} + \int_{ND}^{CK} \frac{\partial A_{area}}{\partial R_d}\ dR_d \tag{16}$$

The integrals were evaluated numerically by dividing the interval between the two treatments into 1000 steps (the same method used for numerical integration of Eqn 7). A partial derivation was estimated at each step in the interval by computing the small finite change in A_{area} with the implemented computer code written by Buckley and Diaz-Espejo (2015*a*). After the integrals were completed, each of them represents an estimate of the absolute contribution of each variable to the total difference in A_{area}. These individual contributions were divided by the difference in A_{area} and multiplied by 100 to yield the percentage contribution of each variable to the variation in A_{area}. A full elaboration of the calculations and equations is presented in Supplementary Protocol S2.

Statistical analyses

Descriptive statistical analyses were performed to assess the ranges of variables and standard errors (SEs). One-way analysis of variance was performed to reveal statistically significant differences across treatments in the studied leaf traits using SPSS 18.0 software (SPSS, Chicago, IL, USA). A principle components analysis was carried out using the 'factoMineR' and 'factoextra' packages in R 3.6.1 (R Foundation for Statistical Computing, Vienna, Austria) to assess the relationship between functional and anatomical traits. Graphics were created, and regressions were performed using OriginPro 8.5 software (OriginLab Corp., Northampton, MA, USA).

Table 1. Leaf gross structure as affected by N, P, K, and B nutrient during seedling stage

Trait	Control	N deficiency	P deficiency	K deficiency	B deficiency
Plant biomass (g)	21.4±1.3a	6.9±1.0bc	5.9±0.8c	9.9±0.9b	9.4±0.7b
Leaf area (cm^2)	299±22a	109±12c	88±3c	192±26b	131±8c
Leaf biomass (g)	1.90±0.11a	0.75±0.13c	0.68±0.03d	1.06±0.10b	1.20±0.08b
LMA (g m^{-2})	64.1±4.2cd	68.3±5.5bc	77.2±1.2b	55.8±2.3d	91.5±1.2a
T_L (μm)	343±7c	354±14c	493±9b	334±2c	549±7a
D_L (g cm^{-3})	0.187±0.012ab	0.193±0.016a	0.157±0.002b	0.167±0.007ab	0.167±0.002ab

Data are mean ± SE of three leaves per treatment. Different letters indicate statistically significant differences (P<0.05) among the treatments. D_L, leaf density; LMA, leaf mass per leaf area; T_L, leaf thickness.

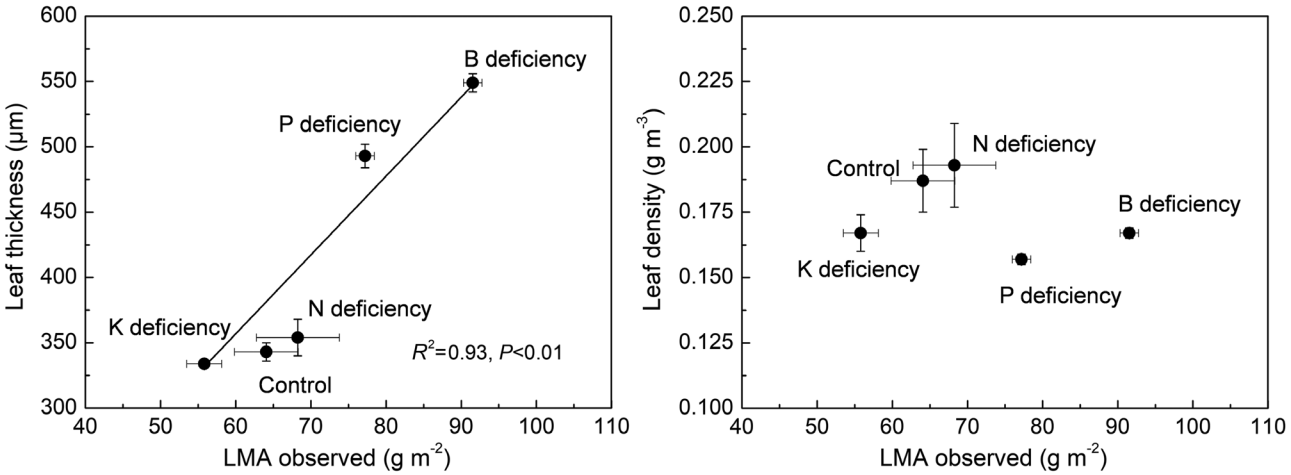

Fig. 2. Relationships between observed leaf mass per area (LMA) and leaf thickness and density. Data are mean ± SE (n=3 plants). The line was fitted using linear regression (significant at P<0.01).

Results

Variation in leaf gross and functional traits under nutrient-deficient conditions

The leaf gross traits were considerably different under nutrient-deficient conditions from under the control condition (CK). The plant biomass and leaf biomass and area significantly decreased under nutrient-deficient conditions, particularly under P and N deficiency (Fig. 1;Table 1).The LMA showed considerable variation, from 55.8 g m^{-2} under K deficiency to 91.5 g m^{-2} under B deficiency. The variation in leaf thickness (T_L) was similar among the five treatments, resulting in a tight correlation between LMA and T_L (Fig. 2). However, leaf density only changed 18.7%, from 0.157 g m^{-3} under P deficiency to 0.193 g m^{-3} under N deficiency, and was not correlated with LMA. Nutrient deficiency decreased leaf vein mass per leaf area (TMA_V) by an average of 6.8% (see Supplementary Table S1).

Leaf functional traits that closely correlated with leaf carbon fixation were considerably changed under nutrient deficiency (Table 2). Both area- and mass-based light-saturated photosynthetic rates were significantly lower under nutrient-deficient conditions. K and B deficiency caused the greatest decreases in the leaf photosynthetic capacity, the main traits of which, including stomatal conductance to H_2O (g_s), mesophyll conductance to CO_2 (g_m), potential electron transport rate at PPFD of 1200 μmol m^{-2} s^{-1} (J_{1200}), and maximum carboxylation rate (V_{cmax}), were reduced by >50%. However, the effect of B deficiency on J_{1200} and V_{cmax} was smaller than that of deficiencies in other nutrients.

We evaluated the average contributions of variables to the observed changes in photosynthetic capacity (Fig. 3). Diffusion (the sum of stomatal and mesophyll conductance) and biochemical factors were found to contribute equally to the decreased leaf photosynthesis under N, P, and K deficiency, whereas 95.3% of the decreased photosynthesis in B-deficient leaves was explained by diffusion limitation. Mesophyll conductance was a greater contributor to controlling CO_2 diffusion in B-, N-, and K-deficient leaves.

Nutrient-mediated shifts in leaf cell- and tissue-scale properties

We estimated the effects of nutrient deficiency on leaf cell- and tissue-scale properties (Table 3). The majority of leaf anatomical traits differed significantly among the treatments. The cell cross-sectional area increased in leaf tissues under nutrient deficiency, specifically the areas of P- and B-deficient leaves were 1.56- to 2.33-fold greater than that of the CK group. Nutrient deficiency increased the perimeter of different tissue cells (+20.1% on average). Leaves with inadequate P and B exhibited elongated palisade and spongy cells with longer cell perimeter and higher cell aspect ratio. However, the increments of epidermal cell perimeter in nutrient-poor leaves (relative to control) were smaller in comparison with the changes of

Table 2. Leaf functional traits as affected by N, P, K and B nutrient during seedling stage

Trait	Control	N deficiency	P deficiency	K deficiency	B deficiency
A_{area} (μmol m^{-2} s^{-1})	13.9±0.3a	8.1±0.2b	7.3±0.5bc	6.4±0.2c	6.8±0.6c
A_{mass} (nmol g^{-1} s^{-1})	217±5a	118±3b	94±6c	115±4b	74±6d
R_d (μmol m^{-2} s^{-1})	1.17±0.10b	1.42±0.22ab	1.34±0.20ab	1.44±0.07ab	1.70±0.04a
g_s (mol m^{-2} s^{-1})	0.156±0.007a	0.123±0.007b	0.095±0.009b	0.073±0.018b	0.064±0.011b
C_i (μmol mol^{-1})	226±4ab	206±9b	197±2b	260±17a	204±15b
g_m (mol m^{-2} s^{-1})	0.235±0.016a	0.165±0.029b	0.196±0.027ab	0.082±0.008c	0.075±0.007c
C_c (μmol mol^{-1})	166±8a	149±15ab	160±3a	180±24a	112±10b
J_{1200} (μmol m^{-2} s^{-1})	222±9a	175±10b	150±18bc	101±5d	199±8ab
V_{cmax} (μmol m^{-2} s^{-1})	134±4a	106±11ab	87±11bc	64±8c	116±11ab

Data are mean ± SE of three leaves per treatment for J_{1200} and V_{cmax}, and four leaves per treatment for A, g_s, C_i, g_m, C_c, and R_d. Different letters indicate statistically significant differences (P<0.05) among the treatments. A_{area}, light-saturated photosynthetic rate per unit leaf area; A_{mass}, light-saturated photosynthetic rate per unit mass; C_c, chloroplastic CO_2 concentration; C_i, intercellular CO_2 concentration; g_m, mesophyll conductance to CO_2; g_s, stomatal conductance to H_2O; J_{1200}, potential electron transport rate at PPFD of 1200 μmol m^{-2} s^{-1}; R_d: day respiration rate; V_{cmax}, maximum carboxylation rate.

Fig. 3. Contributions of individual variables to changes of light-saturated photosynthetic rate per unit leaf area (A_{area}) under N, P, K, and B deficiency when compared with control treatment. The average contributions of stomatal conductance to CO_2 (g_{sc}), mesophyll conductance (g_m), and biochemical limitations (Bio) were estimated according to the method reported by Buckley and Diaz-Espejo (2015*a*). (This figure is available in color at *JXB* online.)

palisade and spongy cells. Nutrient deficiency decreased the number of cells per leaf area, particularly in low P and B leaves, of which the whole cross-sectional cell numbers decreased by 55.3% and 40.3%, respectively.

In most cases, the numbers of spongy and palisade mesophyll cell layers were independent of nutrient deficiency; however, the number of palisade cell layers of B-deficient leaves was 19.3% higher than that of the CK group. P deficiency decreased the air space fraction of the mesophyll cell layers, mainly due to decreased intercellular air space of the spongy layers rather than of the palisade mesophyll layers. Additionally, the air space fraction was affected little by N, K, or B deficiency. Leaves deficient in K had 28.5% lower cell dry-mass densities (ρ_{cell}) than the CK group, whereas N and B deficiency increased ρ_{cell} by 43.9% and 86.2%, respectively. Also, N, P, and B deficiency enhanced the cell wall thickness (T_{cw}) by 1.57-, 2.27-, and 3.97-fold compared with the CK group. K deficiency had a non-significant effect on the T_{cw}. The length of mesophyll exposed to intercellular airspace per cross-sectional area ($l_m/A_{section}$) ranged from 0.036 (P deficiency) to 0.049 μm^{-1} (N and K deficiency). The mesophyll surface area exposed to intercellular airspace per unit leaf area (S_m) was similar under N, P, and K deficiency and in the CK group, but was 31.4% larger under B deficiency. Nutrient deficiency, particularly K deficiency, resulted in a marked decrease in the chloroplast surface area exposed to intercellular air space per leaf area (S_c).

Compositional basis for the variations in LMA

We used the EXACT model, which has a strong ability to explain LMA from the numbers, dimensions, and mass densities of leaf cells and tissues (John *et al.*, 2017), to clarify the compositional basis of nutrient-mediated differences in LMA. The modelled LMA values of rapeseed leaves were similar to those observed under multiple nutrient deficiencies (R^2=0.98, P<0.01; Fig. 4), indicating the good explanatory power of this approach on calculated LMA. By using air space fraction, number of cell layers, estimated cell volume (since this metric is needed in the EXACT model, we estimated it by assuming epidermal cells as cylinders, palisade and spongy mesophyll cells as capsules; see Supplementary Table S3) and ρ_{cell}, we performed a quantitative analysis to identify which factors were important realized determinants of LMA variations between the CK and nutrient-deficiency treatments (Fig. 5). The slightly higher LMA caused by N deficiency was predominantly driven by the increased ρ_{cell} (101.7%), but negatively influenced by vein mass per leaf area (TMA_V, −33.8%). Under P-deficient conditions, the LMA increased, which was mainly attributed to the up-regulated volume of palisade mesophyll cells (CV_{pa}, 45.6%) and spongy mesophyll cells (CV_{sp}, 36.5%). However, the decrease in TMA_V (−27.0%) of P-deficient leaves negatively impacted the increment of LMA. K deficiency slightly decreased LMA by reducing the ρ_{cell} (127.2%) and TMA_V (27.8%). The ρ_{cell} (61.8%), CV_{pa} (17.6%), number of palisade mesophyll layers (NCL_{pa}, 10.5%), and CV_{sp} (8.6%) were the important determinants of the increased LMA of B-deficient leaves.

Table 3. Leaf anatomical traits as affected by N, P, K, and B nutrients during seedling stage

Trait	Control	N deficiency	P deficiency	K deficiency	B deficiency
Cell cross-sectional area (μm^2)					
Upper epidermis	501±26b	556±42b	780±78a	607±78b	788±27a
Lower epidermis	364±28c	287±12d	562±17a	339±19c	468±31b
Palisade mesophyll	950±37b	1179±159b	2217±80a	1114±76b	2042±197a
Spongy mesophyll	724±64b	745±86b	1356±31a	718±35b	1178±35a
Cell perimeter (μm)					
Upper epidermis	84.4±8.6b	95.0±3.9ab	106.1±6.0a	99.3±9.4ab	112.5±3.8a
Lower epidermis	72.6±2.8bc	66.0±2.6c	96.5±1.1a	77.2±1.5b	89.1±3.6a
Palisade mesophyll	125.2±5.2b	142.0±12.2b	201.1±5.6a	139.2±5.9b	199.2±14.1a
Spongy mesophyll	111.0±9.9b	104.9±5.4b	142.8±2.6a	103.7±2.3b	132.2±2.8a
Cell aspect ratio					
Upper epidermis	1.70±0.07ab	2.04±0.11ab	2.07±0.07a	1.99±0.26ab	1.65±0.01b
Lower epidermis	1.71±0.08a	1.77±0.07a	2.00±0.31a	1.70±0.07a	2.01±0.09a
Palisade mesophyll	1.92±0.16b	1.88±0.21b	2.10±0.07b	2.12±0.05b	2.74±0.14a
Spongy mesophyll	1.44±0.05ab	1.42±0.04b	1.52±0.02ab	1.46±0.04ab	1.54±0.04a
Number of cells per leaf area (×10^9 m^{-2})					
Upper epidermis	3.26±0.66a	2.77±0.61a	1.25±0.27b	1.96±0.37ab	1.33±0.27b
Lower epidermis	1.92±0.53ab	1.99±0.36a	0.71±0.17c	1.39±0.13ab	1.08±0.24bc
Palisade mesophyll	2.30±0.35a	2.31±0.25a	1.03±0.20b	2.45±0.41a	1.86±0.40ab
Spongy mesophyll	4.49±0.61a	4.25±0.16a	2.38±0.46b	4.20±0.17a	2.90±0.38b
Mesophyll cells	6.79±0.96a	6.56±0.40a	3.41±0.66b	6.65±0.34a	4.76±0.45b
Whole cross-section	12.0±0.83a	11.3±0.60a	5.37±0.37b	10.0±0.31a	7.17±0.96b
Number of cell layers					
Palisade mesophyll	3.06±0.06b	3.29±0.04b	3.32±0.12b	3.18±0.03b	3.65±0.22a
Spongy mesophyll	4.63±0.13a	4.40±0.28a	4.90±0.65a	4.64±0.18a	4.92±0.21a
Air space fraction (%)					
Palisade mesophyll	26.2±0.81a	25.3±1.01a	25.5±1.46a	25.3±1.72a	23.7±1.89a
Spongy mesophyll	42.3±1.53 a	40.3±1.52a	34.3±1.25b	41.5±2.37a	40.6±2.69a
Mesophyll cell layers	30.6±1.72ab	29.7±1.14ab	27.5±0.26b	30.2±2.15ab	33.4±1.51a
Other traits					
ρ_{cell} (kg m^{-3})	116.3±6.6c	167.4±12.0b	115.6±5.1c	83.2±22.6d	216.6±9.0a
T_{cw} (μm)	0.153±0.006d	0.240±0.018c	0.347±0.015b	0.171±0.018d	0.608±0.036a
$I_m/A_{section}$ (μm^{-1})	0.046±0.001a	0.049±0.001a	0.036±0.001b	0.049±0.002a	0.038±0.001b
S_m (m^{-2} m^{-2})	22.4±0.66b	22.5±1.34b	24.2±0.95b	22.3±0.87b	30.3±1.36a
S_c (m^{-2} m^{-2})	16.3±0.42a	12.8±1.21bc	15.4±0.45ab	11.4±1.38c	13.1±0.75bc

Data are mean ± SE of four leaves per treatment. Different letters indicate statistically significant differences (P<0.05) among the treatments. $I_m/A_{section}$, the length of mesophyll exposed to intercellular airspace per cross-sectional area; ρ_{cell}, cell dry mass density; S_c, chloroplast surface area exposed to intercellular air space per unit leaf area; S_m, mesophyll surface area exposed to intercellular airspace per unit leaf area; T_{cw}, cell wall thickness.

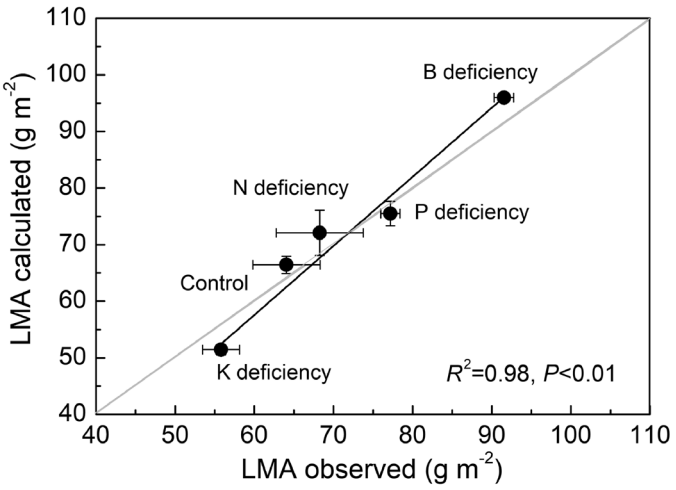

Fig. 4. Observed values for leaf mass per area (LMA) plotted against values predicted by the EXACT model (John *et al.*, 2017). Data are mean ± SE. The black line was fitted using linear regression (significant at P<0.01), and the grey line represents 1:1.

Discussion

Leaf carbon investment strategy for coping with nutrient deficiency is associated with internal distribution of carbon between ρ_{cell} and cellular anatomy

Leaves cope with nutrient depletion by changing both the magnitude and the cellular components of LMA. The results of our sensitivity analysis indicate that the strongest drivers of the changes in LMA under nutrient deficiency were ρ_{cell} and cellular anatomy, including the volumes of palisade and spongy mesophyll cells and the number of palisade mesophyll layers. As suggested by Poorter *et al.* (2009), ρ_{cell} was mainly determined by the cellular chemical composition, including minerals, total non-structural carbohydrates, total structural carbohydrates, organic acids, soluble phenolics, proteins, lignins, and lipids. Therefore, nutrient elements modulate LMA most likely by modulating the flow of carbon into chemical components or cellular structures.

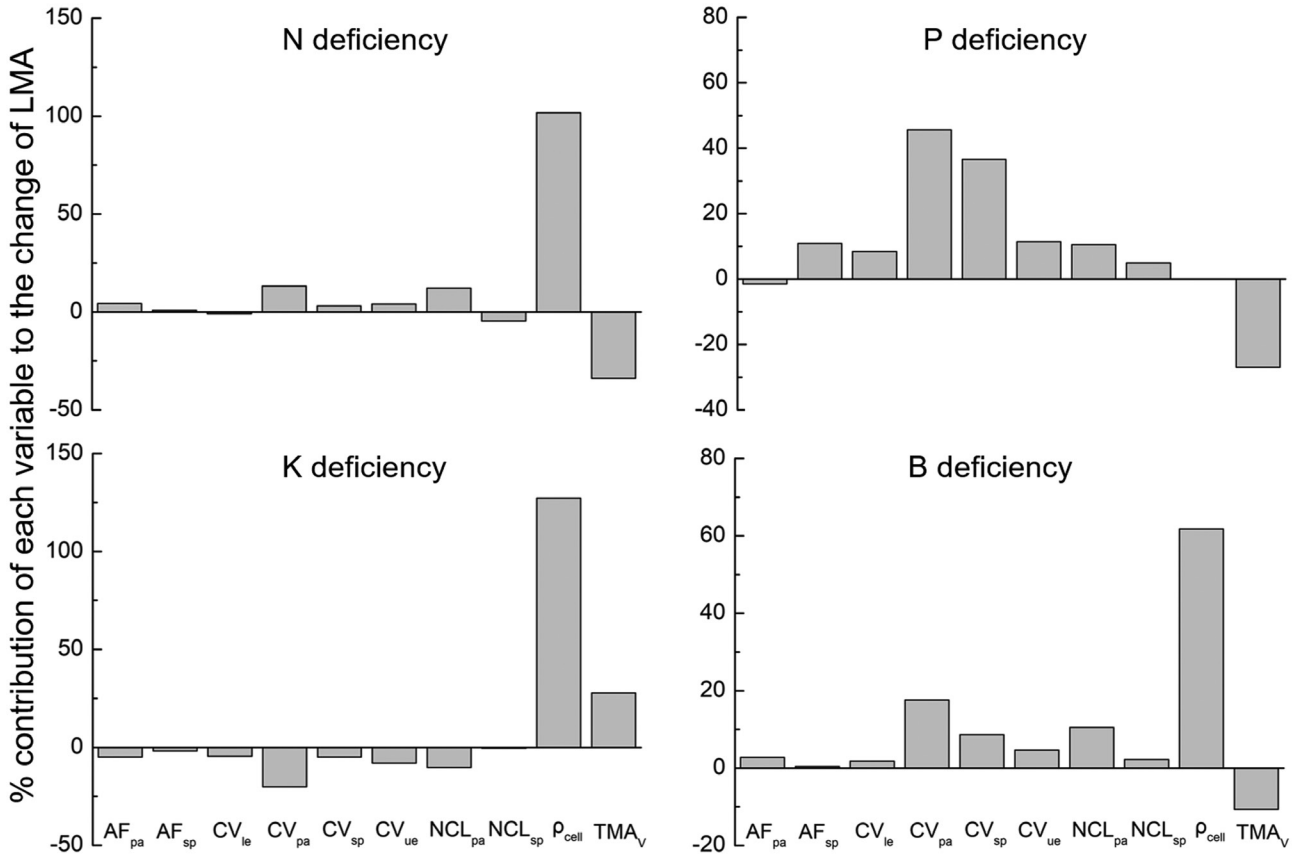

Fig. 5. Partitioning the influence of anatomical and compositional traits on the variations in leaf mass per area (LMA) between nutrient deficiency and control treatment with EXACT model. AF_{pa} and AF_{sp}, air fraction of palisade and spongy mesophyll; CV_{le}, CV_{pa}, CV_{sp}, CV_{ue}, mean cell volume of lower epidermis, palisade mesophyll, spongy mesophyll, and upper epidermis; NCL_{pa} and NCL_{sp}, the number of palisade and spongy mesophyll cell layers; ρ_{cell}, average cell dry mass density; TMA_v, vein mass per leaf area.

In the present study, N and K had a moderate influence on LMA (<15% shifts compared with the control treatment) and ρ_{cell} was the predominant determinant, indicating that N and K are particularly relevant to the allocation of carbon to cellular components (Fig. 2). N deficiency reportedly enhances the investment of carbon in cell wall components such as total structural carbohydrates (Amtmann and Armengaud, 2009; Ali and Golombek, 2016), lignin (Sun *et al.*, 2018), and phenolics (Booker, 2000), which increased the average ρ_{cell}; in contrast, the lowered ρ_{cell} in K-deficient leaves was mainly driven by the decreased accumulation of solutes (Amtmann and Armengaud, 2009). In the case of P deficiency, more carbon was distributed to construct leaves with larger epidermis, palisade, and spongy cells and a lower air fraction of the spongy mesophyll, resulting in LMA up-regulation (Fig. 1). The involvement of P in cell expansion is primarily attributed to the sharply decreased cell number (Table 3), because cell division may be inhibited by lower leaf cytokinin levels (Hare *et al.*, 1997; Wang *et al.*, 2006) and increased callose deposition in low-P leaves (Müller *et al.*, 2015). B-deficient plants invested more carbon to increase leaf chemical compositions (mainly cell wall components) and the average cell volume, with ρ_{cell} and anatomy traits contributing 61.8% and 45.3% of the total increase in LMA, respectively (Fig. 5). These findings suggest that nutrition-mediated shifts in LMA are attributable to the alteration of carbon investment in ρ_{cell} and cellular anatomy, which is of particular relevance to the functions of nutrients.

Among the elements studied, K has a non-structural role, and its deficiency greatly decreased inorganic ions and cellular metabolites (Amtmann and Armengaud, 2009) and eventually the ρ_{cell} and LMA. In contrast, plants suffering from N, P, and B deficiency have tougher leaves (a higher LMA) because of a larger ρ_{cell} (Poorter *et al.*, 2009) and/or cell expansion. Since LMA plays a central role in various plant strategy schemes, future research should scale up the influence of micro components of LMA and comprehensively consider the specific function of limiting nutrients in assigning species' resource-use strategies in an oligotrophic ecosystem.

Functional consequences and causes of nutrition on leaf carbon fixation: the importance of leaf anatomy

Distinct leaf carbon investments in nutrient-poor leaves result in different leaf components (both structural and biochemical) that could be incorporated to influence leaf carbon fixation. One of the primary photosynthetic traits most relevant to a combination of anatomical and biochemical factors is g_m (Lehmeier *et al.*, 2017; Lundgren and Fleming, 2020). In the present study, when diffusional limitation is broken down into

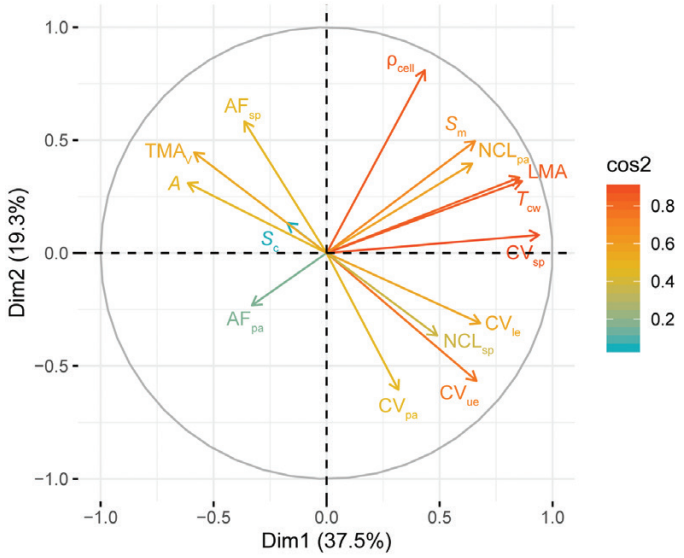

Fig. 6. Principal component analysis of leaf functional and structural traits for rapeseed plants under multiple nutrient deficiencies. The quality of representation of the variables on factor map (cos2) is indicated in different colors. A higher cos2 indicates a good representation of the variable on the principal component. In this case the variable is positioned close to the circumference of the correlation circle. A_{area}, light-saturated photosynthetic rate per unit leaf area; AF_{pa} and AF_{sp}, air fraction of palisade and spongy mesophyll; CV_{le}, CV_{pa}, CV_{sp}, CV_{ue}, mean cell volume of lower epidermis, palisade mesophyll, spongy mesophyll and upper epidermis; NCL_{pa} and NCL_{sp}, the number of palisade and spongy mesophyll cell layers; ρ_{cell}, average cell dry mass density; S_c, chloroplast surface area exposed to intercellular air space per unit leaf area; S_m, mesophyll surface area exposed to intercellular airspace per unit leaf area; T_{cw}, cell wall thickness; TMA_v, vein mass per leaf area. (This figure is available in color at *JXB* online.)

individual variables, the contribution from g_m was larger in N-, K-, and B-deficient leaves (Fig. 3), indicating the pivotal function of nutrients in regulating CO_2 flux within the mesophyll (Xiong and Flexas, 2018; Lu *et al.*, 2019). The distinct changes in S_c and/or T_{cw} might underpin the observed decrease in g_m; nevertheless, the underlying mechanisms that trigger these variations could be diverse depending on different mineral elements. N, K, and B deprivation down-regulated S_c, thus reducing the surface area for CO_2 dissolution to reach the site of carboxylation. Given that the S_m did not synchronously decrease with the S_c or even increased in B-poor leaves (because higher leaf thickness compensated for the decreased $l_m/A_{section}$), the decreased S_c in nutrient-deficient leaves was most likely due to the decreased chloroplast quantity because of accelerated chloroplast degradation (Hall *et al.*, 1972; Lu *et al.*, 2016). In plants undergoing nutrient stress, the degradation of chloroplasts and the recycling of their nutrients is an effective means to ensure growth and delay senescence (Xie *et al.*, 2015). Especially for K^+, which accounted for up to 80% of the cations in the chloroplast stroma, its low concentration in K-starved leaf (see Supplementary Table S4) could not maintain homeostasis and chloroplast development (Schröppel-Meier and Kaiser, 1988), resulting in a more striking decrease in S_c. Additionally, the lower g_m values in N- and B-deprived leaves were related to increased T_{cw}, which is probably attributed to the enhanced carbon flux to the cell wall (Ali and Golombek, 2016) and impaired formation of dimeric B-dRGII pectin complexes (Marschner, 2012), respectively. The role of K in mediating T_{cw} is marginal, but K starvation is known to increase cytoplasmic resistance by enhancing the distance of the chloroplast from the cell walls and between adjacent chloroplasts (Lu *et al.*, 2016). N and B deficiency may also impact cellular resistances along the leaf internal CO_2 diffusion pathway, but to date, their magnitude and relative contributions have never been quantified. Biochemical-based features, such as membranes and aqueous compartments (aquaporins and carbonic anhydrases) and apoplastic metabolism (modifying the physical and chemical composition of the cell wall), could influence g_m, and sometimes their contribution can be even larger than that of leaf anatomy (Tomás *et al.*, 2013; Clemente-Moreno *et al.*, 2019). Nutrient status may influence these biochemical properties (Kanai *et al.*, 2011; Ding *et al.*, 2018), but whether the decrease in g_m is associated with biochemical factors is unknown.

In contrast, a doubling of cell wall thickness in P-deficient leaves resulted in a slight decrease in g_m. This is largely because the key determinant S_c decreased by less than 10% in P-starved leaves. P starvation suppresses the activity of ribonuclease polynucleotide phosphorylase and to some extent reduces P consumption during the degradation of chloroplastidial RNA, which induces a phosphate sparing strategy in low-P plants (Yehudai-Resheff *et al.*, 2007). For cellular resistance, cell wall contributed only 10% of the liquid-phase resistance in rapeseed leaves, whereas most of the resistance was situated in the chloroplast stroma (40–55%; Lu *et al.*, 2016). In this sense, g_m may not be sensitive enough and cannot always be revealed by overt alterations in anatomical components such as cell wall thickness (Lehmeier *et al.*, 2017). If structural traits represent only a small proportion of liquid-phase resistance, then one may not expect that their variations would reveal similar-magnitude changes in g_m while other key determinants (e.g. S_c) do not change much. The possible changes in air channel diameter, connectivity, and tortuosity, and cell wall porosity in P-deficient leaves may also be responsible for the non-synchronous changes between cell wall thickness and g_m (Evans *et al.*, 2009; Lehmeier *et al.*, 2017).

A_{area} and LMA respond co-ordinately under nutrient-poor conditions

It is likely that A_{area} contributes substantially to the plant carbon flow available for leaf establishment under different carbon investment strategies, and that carbon flow has knock-on effects on structural properties, which may, in turn, affect A_{area}. The carbon-investment trade-offs among those anatomical traits may underlie the covariation of A_{area} and LMA. Therefore, by principal component analysis of leaf functional and anatomical traits, we assessed the relationship of A_{area} and LMA and their potential structural basis (Fig. 6). The two principal components (dim 1 and dim 2) explained 56.8% of the variance in the data set. A_{area} was negatively correlated with LMA when the results of all treatments were pooled. This relationship has been regarded as a universality of the leaf economics spectrum across species and communities and is used to interpret leaf resource-use strategies (Wright *et al.*, 2002; Poorter *et al.*, 2009). A_{area}

was found to be positively related to the combination of S_c and the air fraction of the palisade and spongy mesophyll, whereas LMA was most closely related to T_{cw}, the volume of spongy mesophyll cells, and the number of palisade cell layers, which was in close agreement with the observations of Shipley *et al.* (2006). Therefore, under nutrient-stress conditions, LMA is likely to be increased by greater investment of carbon in mesophyll cells, leading to fewer but larger and slightly more tightly arranged cells, a greater number of cell layers, and a thicker cell wall. This is thought to be an adaption to increase leaf lifespan by structural reinforcement under adverse conditions that favour slow tissue turnover (Wright *et al.*, 2002). Although the LMA in K-deficient rapeseed leaves was decreased, the carbon distribution was somewhat similar to those under N, P, and B deficiency, with fewer cells and a slightly greater T_{cw}. Increasing the number of mesophyll cells enhanced A_{area} by manipulating S_c (Ren *et al.*, 2019; Lundgren and Fleming, 2020). However, S_c was not affected by the smaller number of cells in nutrient-poor leaves because S_m remained unchanged (N, P, K deficiency) or even increased (B deficiency). Therefore, the decreased S_c was likely due to the decreased investment of carbon needed to maintain chloroplast quantity. Additionally, the thicker cell wall in nutrient-poor leaves enhanced cell wall resistance to CO_2 diffusion and decreased A_{area} (Tomás *et al.*, 2013). Therefore, we confirmed the hypothesis that leaves with a low mineral nutrient content exhibit reduced carbon fixation (lower A_{area}) and tend to invest more carbon to produce larger cells with a thicker cell wall and smaller S_c, which decreases mesophyll conductance and causes feedback limitation of A_{area}.

Our data provide insight into the importance of mineral nutrients in leaf trait trade-offs by considering the compositional basis of two key attributes of the leaf economics spectrum. Moreover, the results reveal a conserved coordination between A_{area} and LMA that is independent of nutrient-specific limitations. This provides direct evidence that the microstructural carbon distribution is a fundamental determinant of LMA and its covariation with A_{area}. Leaf cell and tissue traits should be considered underlying determinants of variations in A_{area} and LMA and their relevance under multiple environments, especially when their covariation is weakened, or the relationship does not map to the leaf carbon-use strategy (Peguero-Pina *et al.*, 2017; Anderegg *et al.*, 2018; Nadal *et al.*, 2018). Our analysis also suggests potential factors (e.g. cell dry mass density and cell volume) in the leaf economics spectrum that may enhance our understanding of leaf internal carbon investment and the observed trade-offs.

Conclusions

In nutrient-poor habitats, plants have a weaker carbon fixation capacity (lower A_{area}) and produce less carbon to flow into the leaf. However, LMA responds diversely in oligotrophic habitats, being either increased or decreased. Our results show that the variations in LMA are largely dependent on nutrient-mediated shifts in the cell- and tissue-level carbon distribution between ρ_{cell} and cellular anatomy. N, P, and B deficiencies tend to increase LMA by enhancing carbon allocation to cellular chemical components (increasing ρ_{cell}) and/or to support cell expansion, whereas decreased cellular solutes (reducing ρ_{cell}) could be the uppermost reason for the down-regulation of LMA in K-starved leaves. Despite these striking differences in microstructural carbon investment, leaves with insufficient mineral nutrients tend to invest more carbon in non-photosynthetic tissues to produce fewer but larger cells with a thicker cell wall and smaller S_c, leading to feedback regulation of A_{area}. Therefore, nutrient-induced variations in carbon assimilation and internal distribution could respond co-ordinately to balance the leaf carbon economy.

Supplementary data

The following supplementary data are available at *JXB* online.

Fig. S1. Relationship between the actual photochemical efficiency of photosystem II (Φ_{PSII}) and Φ_{CO_2}.

Table S1. Leaf biomass, area, leaf mass per area, and vein mass per leaf area as affected by nutrient deficiency during seedling stage of 2019–2020 growing season.

Table S2. Sensitivity analysis of the relative importance of anatomical or compositional variables to LMA variation resulting from ±5% of the TMA_V deviation.

Table S3. Cell volume as affected by nutrient deficiency during seedling stage.

Table S4. Leaf nitrogen (N), phosphorus (P), potassium (K), and boron (B) concentration as affected by nutrient deficiency during seedling stage.

Protocol S1. Measurements of vein mass per leaf area.

Protocol S2. Analysis of partitioning changes in A_{area}.

Acknowledgements

This work was financially supported by National Natural Science Foundation of China (31801933), the National Key Research and Development Program of China (2018YFD0200900), and the Fundamental Research Funds for the Central Universities (2662018PY077). The authors thank Dr Thomas N. Buckley and Dr Grace P. John for their help in applying mathematic models, Dr Yong Li for his suggestions on improving the manuscript.

Conflict of interest

The authors declare that they have no conflict of interest.

Data availability

All data supporting the findings of this study are available within the paper and within its supplementary materials published online.

References

Ali ZI, Golombek SD. 2016. Effect of drought and nitrogen availability on osmotic adjustment of five pearl millet cultivars in the vegetative growth stage. Journal of Agronomy and Crop Science **202**, 433–444.

Alloway BJ. 2008. Micronutrient deficiencies in global crop production. Dordrecht: Springer Science & Business Media.

Amtmann A, Armengaud P. 2009. Effects of N, P, K and S on metabolism: new knowledge gained from multi-level analysis. Current Opinion in Plant Biology **12**, 275–283.

Anderegg LDL, Berner LT, Badgley G, Sethi ML, Law BE, HilleRisLambers J. 2018. Within-species patterns challenge our understanding of the leaf economics spectrum. Ecology Letters **21**, 734–744.

Battie-Laclau P, Laclau JP, Beri C, Mietton L, Muniz MR, Arenque BC, De Cassia Piccolo M, Jordan-Meille L, Bouillet JP, Nouvellon Y. 2014. Photosynthetic and anatomical responses of *Eucalyptus grandis* leaves to potassium and sodium supply in a field experiment. Plant, Cell & Environment **37**, 70–81.

Blonder B, Violle C, Bentley LP, Enquist BJ. 2011. Venation networks and the origin of the leaf economics spectrum. Ecology Letters **14**, 91–100.

Booker FL. 2000. Influence of carbon dioxide enrichment, ozone and nitrogen fertilization on cotton (*Gossypium hirsutum* L.) leaf and root composition. Plant, Cell & Environment **23**, 573–583.

Buckley TN, Diaz-Espejo A. 2015*a*. Partitioning changes in photosynthetic rate into contributions from different variables. Plant, Cell & Environment **38**, 1200–1211.

Buckley TN, Diaz-Espejo A. 2015*b*. Reporting estimates of maximum potential electron transport rate. New Phytologist **205**, 14–17.

Chatelet DS, Clement WL, Sack L, Donoghue MJ, Edwards EJ. 2013. The evolution of photosynthetic anatomy in *Viburnum* (Adoxaceae). International Journal of Plant Sciences **174**, 1277–1291.

Clemente-Moreno MJ, Gago J, Díaz-Vivancos P, Bernal A, Miedes E, Bresta P, Liakopoulos G, Fernie AR, Hernández JA, Flexas J. 2019. The apoplastic antioxidant system and altered cell wall dynamics influence mesophyll conductance and the rate of photosynthesis. The Plant Journal **99**, 1031–1046.

Dible WT, Truog E, Berger KC. 1954. Boron determination in soils and plants. Analytical Chemistry **26**, 418–421.

Ding L, Lu Z, Gao L, Guo S, Shen Q. 2018. Is nitrogen a key determinant of water transport and photosynthesis in higher plants upon drought stress? Frontiers in Plant Science **9**, 1143.

Duursma RA. 2015. Plantecophys – an R package for analysing and modeling leaf gas exchange data. PLoS One **10**, e0143346.

Ellsworth DS, Crous KY, Lambers H, Cooke J. 2015. Phosphorus recycling in photorespiration maintains high photosynthetic capacity in woody species. Plant, Cell & Environment **38**, 1142–1156.

Evans JR, Kaldenhoff R, Genty B, Terashima I. 2009. Resistances along the CO_2 diffusion pathway inside leaves. Journal of Experimental Botany **60**, 2235–2248.

Farquhar GD, von Caemmerer S, Berry JA. 1980. A biochemical model of photosynthetic CO_2 assimilation in leaves of C_3 species. Planta **149**, 78–90.

Hall JD, Barr R, Al-Abbas AH, Crane FL. 1972. The ultrastructure of chloroplasts in mineral-deficient maize leaves. Plant Physiology **50**, 404–409.

Hare PD, Cress WA, van Staden JV. 1997. The involvement of cytokinins in plant responses to environmental stress. Plant Growth Regulation **23**, 79–103.

Harley PC, Loreto F, Di Marco G, Sharkey TD. 1992. Theoretical considerations when estimating the mesophyll conductance to CO_2 flux by analysis of the response of photosynthesis to CO_2. Plant Physiology **98**, 1429–1436.

Harwood R, Goodman E, Gudmundsdottir M, Huynh M, Musulin Q, Song M, Barbour MM. 2020. Cell and chloroplast anatomical features are poorly estimated from 2D cross-sections. New Phytologist **225**, 2567–2578.

Jákli B, Tavakol E, Tränkner M, Senbayram M, Dittert K. 2017. Quantitative limitations to photosynthesis in K deficient sunflower and their implications on water-use efficiency. Journal of Plant Physiology **209**, 20–30.

John GP, Scoffoni C, Buckley TN, Villar R, Poorter H, Sack L. 2017. The anatomical and compositional basis of leaf mass per area. Ecology Letters **20**, 412–425.

John GP, Scoffoni C, Sack L. 2013. Allometry of cells and tissues within leaves. American Journal of Botany **100**, 1936–1948.

Kanai S, Moghaieb RE, Ei-Shemy HA, Panigrahi R, Mohapatra PK, Ito J, Nguyen NT, Saneoka H, Fujita K. 2011. Potassium deficiency affects water status and photosynthetic rate of the vegetative sink in green house tomato prior to its effects on source activity. Plant Science **180**, 368–374.

Lancashire PD, Bleiholder H, Boom T, Langelüddeke P, Stauss R, Weber E, Witzenberger A. 1991. A uniform decimal code for growth stages of crops and weeds. Annals of Applied Biology **119**, 561–601.

Lehmeier C, Pajor R, Lundgren MR, *et al*. 2017. Cell density and airspace patterning in the leaf can be manipulated to increase leaf photosynthesis capacity. The Plant Journal **92**, 981–994.

Li Y, Gao Y, Xu X, Shen Q, Guo S. 2009. Light-saturated photosynthetic rate in high-nitrogen rice (*Oryza sativa* L.) leaves is related to chloroplastic CO_2 concentration. Journal of Experimental Botany **60**, 2351–2360.

Li YS, Lu JW, Liao X, Zou J. 2011. Effects of phosphorus application rate on yield and fertilizer – phosphorus utilization efficiency in rapeseed. Chinese Journal of Oil Crop Sciences **33**, 52–56.

Liu GD, Dong XC, Liu LC, Wu LS, Peng SA, Jiang CC. 2014. Boron deficiency is correlated with changes in cell wall structure that lead to growth defects in the leaves of navel orange plants. Scientia Horticulturae **176**, 54–62.

Lu Z, Lu J, Pan Y, Lu P, Li X, Cong R, Ren T. 2016. Anatomical variation of mesophyll conductance under potassium deficiency has a vital role in determining leaf photosynthesis. Plant, Cell & Environment **39**, 2428–2439.

Lu Z, Xie K, Pan Y, Ren T, Lu J, Wang M, Shen Q, Guo S. 2019. Potassium mediates coordination of leaf photosynthesis and hydraulic conductance by modifications of leaf anatomy. Plant, Cell & Environment **42**, 2231–2244.

Lundgren MR, Fleming AJ. 2020. Cellular perspectives for improving mesophyll conductance. The Plant Journal **101**, 845–857.

Marschner H. 2012. Marschner's mineral nutrition of higher plants. Academic Press.

Müller J, Toev T, Heisters M, Teller J, Moore KL, Hause G, Dinesh DC, Bürstenbinder K, Abel S. 2015. Iron-dependent callose deposition adjusts root meristem maintenance to phosphate availability. Developmental Cell **33**, 216–230.

Nadal M, Flexas J, Gulías J. 2018. Possible link between photosynthesis and leaf modulus of elasticity among vascular plants: a new player in leaf traits relationships? Ecology Letters **21**, 1372–1379.

Nelson EA, Sage TL, Sage RF. 2005. Functional leaf anatomy of plants with crassulacean acid metabolism. Functional Plant Biology **32**, 409–419.

Orlovius K. 2003. Oilseed rape. Fertilizing for high yield and quality. IPI Bulletin No. 16. Basel: International Potash Institute.

Peguero-Pina JJ, Sisó S, Flexas J, Galmés J, García-Nogales A, Niinemets Ü, Sancho-Knapik D, Saz MÁ, Gil-Pelegrín E. 2017. Cell-level anatomical characteristics explain high mesophyll conductance and photosynthetic capacity in sclerophyllous Mediterranean oaks. New Phytologist **214**, 585–596.

Poorter H, Niinemets U, Poorter L, Wright IJ, Villar R. 2009. Causes and consequences of variation in leaf mass per area (LMA): a meta-analysis. New Phytologist **182**, 565–588.

Ren T, Lu JW. 2016. Integrated nitrogen management strategy for winter oilseed rape (*Brassica napus* L.) in China. Scientia Agricultura Sinica **49**, 3506–3521.

Ren T, Weraduwage SM, Sharkey TD. 2019. Prospects for enhancing leaf photosynthetic capacity by manipulating mesophyll cell morphology. Journal of Experimental Botany **70**, 1153–1165.

Sack L, Cowan P, Jaikumar N, Holbrook N. 2003. The 'hydrology' of leaves: co-ordination of structure and function in temperate woody species. Plant, Cell & Environment **26**, 1343–1356.

Sardans J, Peñuelas J. 2015. Potassium: a neglected nutrient in global change. Global Ecology and Biogeography **24**, 261–275.

Schröppel-Meier G, Kaiser WM. 1988. Ion homeostasis in chloroplasts under salinity and mineral deficiency. Plant Physiology **87**, 822–827.

Shipley B, Lechowicz MJ, Wright I, Reich PB. 2006. Fundamental trade-offs generating the worldwide leaf economics spectrum. Ecology **87**, 535–541.

Sun Q, Liu X, Yang J, Liu W, Du Q, Wang H, Fu C, Li WX. 2018. MicroRNA528 affects lodging resistance of maize by regulating lignin biosynthesis under nitrogen-luxury conditions. Molecular Plant **11**, 806–814.

Syvertsen J, Lloyd J, McConchie C, Kriedemann P, Farquhar G. 1995. On the relationship between leaf anatomy and CO_2 diffusion through the mesophyll of hypostomatous leaves. Plant, Cell & Environment **18**, 149–157.

Terashima I, Hanba YT, Tholen D, Niinemets Ü. 2011. Leaf functional anatomy in relation to photosynthesis. Plant Physiology **155**, 108–116.

Thain J. 1983. Curvature correction factors in the measurement of cell surface areas in plant tissue. Journal of Experimental Botany **34**, 87–94.

Thomas RL, Sheard RW, Moyer JR. 1967. Comparison of conventional and automated procedures for nitrogen, phosphorus, and potassium analysis of plant material using a single digestion. Agronomy Journal **59**, 240–243.

Tomás M, Flexas J, Copolovici L, Galmés J, Hallik L, Medrano H, Ribas-Carbó M, Tosens T, Vislap V, Niinemets Ü. 2013. Importance of leaf anatomy in determining mesophyll diffusion conductance to CO_2 across species: quantitative limitations and scaling up by models. Journal of Experimental Botany **64**, 2269–2281.

Tosens T, Niinemets Ü, Westoby M, Wright IJ. 2012. Anatomical basis of variation in mesophyll resistance in eastern Australian sclerophylls: news of a long and winding path. Journal of Experimental botany **63**, 5105–5119.

Tränkner M, Tavakol E, Jákli B. 2018. Functioning of potassium and magnesium in photosynthesis, photosynthate translocation and photoprotection. Physiologia Plantarum **163**, 414–431.

Valentini R, Epron D, Angelis Pd, Matteucci G, Dreyer E. 1995. In situ estimation of net CO_2 assimilation, photosynthetic electron flow and photorespiration in Turkey oak (*Q. cerris* L.) leaves: diurnal cycles under different levels of water supply. Plant, Cell & Environment **18**, 631–640.

Vile D, Garnier É, Shipley B, *et al.* 2005. Specific leaf area and dry matter content estimate thickness in laminar leaves. Annals of Botany **96**, 1129–1136.

Villar R, Ruiz-Robleto J, Ubera JL, Poorter H. 2013. Exploring variation in leaf mass per area (LMA) from leaf to cell: an anatomical analysis of 26 woody species. American Journal of Botany **100**, 1969–1980.

Wang XM, Yi KK, Tao Y, Wang F, Wu ZC, Jiang DA, Chen X, Zhu LH, Wu P. 2006. Cytokinin represses phosphate-starvation response through increasing of intracellular phosphate level. Plant Cell & Environment **29**, 1924–1935.

Warren C. 2006. Estimating the internal conductance to CO_2 movement. Functional Plant Biology **33**, 431–442.

Witkowski ET, Lamont BB. 1991. Leaf specific mass confounds leaf density and thickness. Oecologia **88**, 486–493.

Wright IJ, Reich PB, Westoby M, *et al.* 2004. The worldwide leaf economics spectrum. Nature **428**, 821–827.

Wright IJ, Westoby M, Reich PB. 2002. Convergence towards higher leaf mass per area in dry and nutrient-poor habitats has different consequences for leaf life span. Journal of Ecology **90**, 534–543.

Xie KL, Lu ZF, Pan YH, Gao LM, Hu P, Wang M, Guo SW. 2020. Leaf photosynthesis is mediated by the coordination of nitrogen and potassium: the importance of anatomical-determined mesophyll conductance to CO_2 and carboxylation capacity. Plant Science **290**, 110267.

Xie Q, Michaeli S, Peled-Zehavi H, Galili G. 2015. Chloroplast degradation: one organelle, multiple degradation pathways. Trends in Plant Science **20**, 264–265.

Xiong D, Flexas J. 2018. Leaf economics spectrum in rice: leaf anatomical, biochemical, and physiological trait trade-offs. Journal of Experimental Botany **69**, 5599–5609.

Xiong D, Liu X, Liu L, Douthe C, Li Y, Peng S, Huang J. 2015. Rapid responses of mesophyll conductance to changes of CO_2 concentration, temperature and irradiance are affected by N supplements in rice. Plant, Cell & Environment **38**, 2541–2550.

Xiong D, Wang D, Liu X, Peng S, Huang J, Li Y. 2016. Leaf density explains variation in leaf mass per area in rice between cultivars and nitrogen treatments. Annals of Botany **117**, 963–971.

Yehudai-Resheff S, Zimmer SL, Komine Y, Stern DB. 2007. Integration of chloroplast nucleic acid metabolism into the phosphate deprivation response in *Chlamydomonas reinhardtii*. The Plant Cell **19**, 1023–1038.

Zhao D, Oosterhuis DM. 2002. Cotton carbon exchange, nonstructural carbohydrates, and boron distribution in tissues during development of boron deficiency. Field Crops Research **78**, 75–87.